# We are IntechOpen, the world's leading publisher of Open Access books Built by scientists, for scientists

**4,800**
Open access books available

**122,000**
International authors and editors

**135M**
Downloads

Our authors are among the

**154**
Countries delivered to

**TOP 1%**
most cited scientists

**12.2%**
Contributors from top 500 universities

CLARIVATE ANALYTICS BOOK CITATION INDEX INDEXED

WEB OF SCIENCE™

Selection of our books indexed in the Book Citation Index in Web of Science™ Core Collection (BKCI)

## Interested in publishing with us?
## Contact book.department@intechopen.com

Numbers displayed above are based on latest data collected.
For more information visit www.intechopen.com

# 12

# Self-Similar Hydrodynamics with Heat Conduction

Masakatsu Murakami
*Institute of Laser Engineering, Osaka University*
*Japan*

## 1. Introduction

### 1.1 Dimensional analysis and self-similarity

Dimensional and similarity theory provides one with the possibility of prior qualitative-theoretical analysis and the choice of a set for characteristic dimensionless parameters. The theory can be applied to the consideration of quite complicated phenomena and makes the processing of experiments much easier. What is more, at present, the competent setting and processing of experiments is inconceivable without taking into account dimensional and similarity reasoning. Sometimes at the initial stage of investigation of certain complicated phenomena, dimensional and similarity theory is the only possible theoretical method, though the possibilities of this method should not be overestimated. The combination of similarity theory with considerations resulting from experiments or mathematical operations can sometimes lead to significant results. Most often dimensional and similarity theory is very useful for theoretical as well for practical use. All the results obtained with the help of this theory can be obtained quite easily and without much trouble.

A phenomenon is called self-similar if the spatial distributions of its properties at various moments of time can be obtained from one another by a similarity transformation. Establishing self-similarity has always represented progress for a researcher: self-similarity has simplified computations and the representation of the characteristics of phenomena under investigation. In handling experimental data, self-similarity has reduced what would seem to be a random cloud of empirical points so as to lie on a single curve of surface, constructed using self-similar variables chosen in some special way. Self-similarity enables us to reduce its partial differential equations to ordinary differential equations, which substantially simplifies the research. Therefore with the help of self-similar solutions researchers have attempted to find the underlying physics. Self-similar solutions also serve as standards in evaluating approximate methods for solving more complicated problems.

Scaling laws, which are obtained as a result of the dimensional analysis and other methods, play an important role for understanding the underlying physics and applying them to practical systems. When constructing a full-scale system in engineering, numerical simulations will be first made in most cases. Its feasibility should be then demonstrated experimentally with a reduced-scale system. For astrophysical studies, for instance, such scaling considerations are indispensable and play a decisive role in designing laboratory experiments. Then one should know how to design such a miniature system and how to

judge whether two experimental results in different scales are hydrodynamically equivalent or similar to each other. Lie group analysis (Lie, 1970), which is employed in the present chapter, is not only a powerful method to seek self-similar solutions of partial differential equations (PDE) but also a unique and most adequate technique to extract the group invariance properties of such a PDE system. Lig group analysis and dimensional analysis are useful methods to find self-similar solutions in a complementary manner.

An instructive example of self-similarity is given by an idealized problem in the mathematical theory of linear heat conduction: Suppose that an infinitely stretched planar space ($-\infty < x < \infty$) is filled with a heat-conducting medium. At the initial instant $t = 0$ and at the origin of the coordinate $x = 0$, a finite amount of heat $E$ is supplied instantaneously. Then the propagation of the temperature $\Theta$ is described by

$$\frac{\partial \Theta}{\partial t} = \kappa \frac{\partial^2 \Theta}{\partial x^2}, \tag{1}$$

where $\kappa$ is the constant heat diffusivity of the medium. Then the temperature $\Theta$ at an arbitrary time $t$ and distance from the origin $x$ is given by

$$\Theta = \frac{E}{c\sqrt{4\pi\kappa t}} \exp\left(-\frac{x^2}{4\kappa t}\right), \tag{2}$$

where $c$ is the specific heat of the medium. As a matter of fact, it is confirmed with the solution (2) that the integrated energy over the space is kept constant regardless of time:

$$\int_{-\infty}^{\infty} c\,\Theta(x,t)dx = E \tag{3}$$

The structure of Eq. (2) is instructive: There exist a temperature scale $\Theta_0(t)$ and a linear scale $x_0(t)$, both depending on time,

$$\Theta_0(t) = \frac{E}{c\sqrt{4\pi\kappa t}}, \quad x_0(t) = \sqrt{\kappa t}, \tag{4}$$

such that the spatial distribution of temperature, when expressed in these scales, ceases to depend on time at least in appearance:

$$\frac{\Theta}{\Theta_0} = f(\xi), \quad f(\xi) = \exp\left(-\frac{\xi^2}{4}\right), \quad \xi = \frac{x}{x_0}. \tag{5}$$

Suppose that we are faced with a more complex problem of mathematical physics in two independent variables $x$ and $t$, requiring the solution of a system of partial differential equations on a variable $u(x,t)$ of the phenomenon under consideration. In this problem, self-similarity means that we can choose variable scales $u_0(t)$ and $x_0(t)$ such that in the new scales, $u(x,t)$ can be expressed by functions of one variable:

$$u = u_0(t)U(\xi), \quad \xi = x/x_0(t) \tag{6}$$

The solution of the problem thus reduces to the solution of a system of ordinary differential equations for the function $U(\xi)$.

At a certain point of analysis, dimensional consideration called Π-theorem plays a crucial role in a complementary manner to the self-similar method. Suppose we have some relationship defining a quantity $a$ as a function of $n$ parameters $a_1, a_2, \dots, a_n$:

$$a = f(a_1, a_2, \dots\ a_n)\,. \tag{7}$$

If this relationship has some physical meaning, Eq. (7) must reflect the clear fact that although the numbers $a_1, a_2, \dots, a_n$ express the values of corresponding quantities in a definite system of units of measurement, the physical law represented by this relation does not depend on the arbitrariness in the choice of units. To explain this, we shall divide the quantities $a, a_1, a_2, \dots\ a_n$ into two groups. The first group, $a_1,\ \dots\ a_k$, includes the governing quantities with independent dimensions (for example, length, mass, and time). The second group, $a, a_{k+1}, \dots\ a_n$, contains quantities whose dimensions can be expressed in terms of dimensions of the quantities of the first group. Thus, for example, the quantity $a$ has the dimensions of the product $a_1^p a_2^q \cdots a_k^r$, the quantity $a_{k+1}$ has the dimensions of the product $a_1^{p_{k+1}} a_2^{q_{k+1}} \cdots\ a_k^{r_{k+1}}$, etc. The exponents $p, q, \dots$ are obtained by a simple arithmetic. Thus the quantities,

$$\Pi = \frac{a}{a_1^p a_2^q \cdots a_k^r},\quad \Pi_1 = \frac{a_{k+1}}{a_1^{p_{k+1}} a_2^{q_{k+1}} \cdots\ a_k^{r_{k+1}}}\,,\ \ .\ .\ .\ ,\ \ \Pi_{n-k} = \frac{a_n}{a_1^{p_n} a_2^{q_n} \cdots\ a_k^{r_n}} \tag{8}$$

turn out to be dimensionless, so that their values do not depend how one choose the units of measurement. This fact follows that the dimensionless quantities can be expressed in the form,

$$\Pi = \Phi(\Pi_1, \Pi_2, \dots, \Pi_{n-k})\,, \tag{9}$$

where no dimensional quantity is contained. What should be stressed is that in the original relation (7), $n+1$ dimensional quantities $a, a_1, a_2, \dots, a_n$ are connected, while in the reduced relation (9), $n-k+1$ dimensionless quantities $\Pi,\ \Pi_1, \Pi_2, \dots, \Pi_{n-k}$ are connected with $k$ quantities being reduced from the original relation.

We now apply dimensional analysis to the heat conduction problem considered above. Below we shall use the symbol [a] to give its dimension, as Maxwell first introduced, in terms of the unit symbols for length, mass, and time by the letters $L$, $M$, and $T$, respectively. For example, velocity $v$ has its dimension $[v] = L/T$. Then the physical quantities describing the present system have following dimensions,

$$[x] = L,\ \ [t] = T,\ \ [\kappa] = L^2T^{-1},\ \ \ [E] = ML^2T^{-2},\ \ [c\,\Theta] = ML^3T^{-2}. \tag{10}$$

From Eq. (10), in which five dimensional quantities ($n+1=5$) under the three principal dimensions ($k=3$ for $L$, $M$, and $T$), one can construct the following dimensionless system with two dimensionless parameters Π and $\xi$ ($=\Pi_1$):

$$\Pi = f(\xi),\quad \Pi = \frac{c\,\Theta\sqrt{\kappa t}}{E}\,,\quad \xi = \frac{x}{\sqrt{\kappa t}}\,, \tag{11}$$

where $f$ is unknown function. Substituting Eq. (11) for Eq. (1), one obtains,

$$f'' + \frac{1}{2}(f + \xi f') = 0\,, \tag{12}$$

where the prime denotes the derivative with respect to $\xi$; also the transform relation from partial to ordinary derivatives

$$\frac{\partial f(\xi)}{\partial t} = -\frac{\xi}{2t} f'(\xi), \quad \frac{\partial f(\xi)}{\partial x} = \frac{1}{\sqrt{\kappa t}} f'(\xi), \tag{13}$$

are used. With the help of the boundary condition, $f'(0) = 0$, and Eq. (3), Eq. (12) is integrated to give

$$f(\xi) = \frac{1}{\sqrt{4\pi}} \exp\left(-\frac{\xi^2}{4}\right). \tag{14}$$

Thus Eqs. (11) and (14) reproduce the solution of the problem, Eq. (2).
What is described above is the simple and essential scenario of the approach in terms of self-similar solution and dimensional analysis, more details of which can be found, for example, in Refs. (Lie, 1970; Barenblatt, 1979; Sedov, 1959; Zel'dovich & Raizer, 1966). In the following subsections, we show three specific examples with new self-similar solutions, as reviews of previously published papers for readers' further understanding how to use the dimensional analysis and to find self-similar solutions: The first is on plasma expansion of a limited mass into vacuum, in which two fluids composed of cold ions and thermal electrons expands via electrostatic field (Murakami et al, 2005). The second is on laser-driven foil acceleration due to nonlinear heat conduction (Murakami et al, 2007). Finally, the third is an astrophysical problem, in which self-gravitation and non-linear radiation heat conduction determine the temporal evolution of star formation process in a self-organizing manner (Murakami et al, 2004).

## 2. Isothermally expansion of laser-plasma with limited mass

### 2.1 Introduction

Plasma expansion into a vacuum has been a subject of great interest for its role in basic physics and its many applications, in particular, its use in lasers. The applied laser parameter spans a wide range, $10^{10} \leq \hat{I}_L \hat{\lambda}_L^2 \leq 10^{19}$, where $\hat{I}_L$ is the laser intensity in the units of W/cm$^2$ and $\hat{\lambda}_L$ is the laser wavelength normalized by 1 $\mu m$. For $\hat{I}_L \hat{\lambda}_L^2 \geq 10^{14}$, generation of fast ions is governed by hot electrons with an increase in $\hat{I}_L \hat{\lambda}_L^2$. In this subsection, we focus on rather lower intensity range, $10^{10} \leq \hat{I}_L \hat{\lambda}_L^2 \leq 10^{14}$, where the effect of hot electrons is negligibly small and background cold electrons can be modeled by one temperature. Typical examples of applications for this range are laser driven inertial confinement fusion (Murakami et al., 1995; Murakami & Iida, 2002) and laser-produced plasma for an extreme ultra violet (EUV) light source (Murakami et al, 2006). As a matter of fact, the experimental data employed below for comparison with the analytical model were obtained for the EUV study. Theoretically, this topic had been studied only through hydrodynamic models until the early 1990s. In such theoretical studies, a simple planar (SP) self-similar solution has often been used (Gurevich et al, 1966). In the SP model, a semi-infinitely stretched planar plasma is considered, which is initially at rest with unperturbed density $\rho_0$. At $t = 0$, a rarefaction wave is launched at the edge to penetrate at a constant sound speed $c_s$ into the unperturbed uniform plasma being accompanied with an isothermal expansion. The density

and velocity profiles of the expansion are given by (Landau & Lifshitz, 1959) $\rho = \rho_0 \exp[-(1 + \mathrm{x}/\, c_s t\ \mathrm{cst})]$ and $v = c_s + x/t$, respectively. The solution is indeed quite useful when using relatively short laser pulses or thick targets such that the density scale can be kept constant throughout the process.

However, in actual laser-driven plasmas, a shock wave first penetrates the unperturbed target instead of the rarefaction wave. Once this shock wave reaches the rear surface of a finite-sized target and the returning rarefaction wave collides with the penetrating rarefaction wave, the entire region of the target begins to expand, and thus the target disintegration sets in. If the target continues to be irradiated by the laser even after the onset of target disintegration, the plasma expansion and the resultant ion energy spectrum are expected to substantially deviate from the physical picture given by the SP solution. Figure 1 demonstrates a simplified version of the physical picture mentioned above with temporal evolution of the density profile obtained by hydrodynamic simulation for an isothermal expansion. A spherical target with density and temperature profiles being uniform is employed as an example. In Fig. 1, the density is always normalized to unity at the center, and the labels assigned to each curve denote the normalized time $t/(R_0 c_s)$, where $R_0$ is the initial radius. The horizontal Lagrange coordinate is normalized to unity at the plasma edge. It can be discerned from Fig. 1 that the profile rapidly develops in the early stage for $t/(R_0 c_s) \leq 1$. After the rarefaction wave reflects at the center, the density distribution asymptotically approaches its final self-similar profile (the thick curve with label "$\infty$"), which is expressed in the Gaussian form, $\rho \propto \exp[-(r/R)^2]$ as will be derived below. The initial and boundary conditions employed in Fig. 1 are substantially simplified such that the laser-produced shock propagation and resultant interactions with the rarefaction wave are not described. However, the propagation speeds of the shock and rarefaction waves are always in the same order as the sound speed $c_s$ of the isothermally expanding plasma. Therefore the physical picture shown in Fig. 1 is expected to be qualitatively valid also for

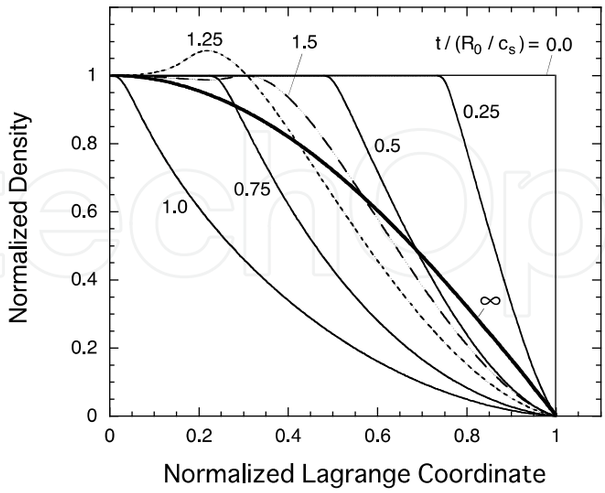


Fig. 1. Temporal evolution of the density profile of a spherical isothermal plasma, which is normalized by that at the center; $R_0$ and $c_s$ are the initial radius and the sound speed, respectively. After the rarefaction wave reflects at the center, the density distribution asymptotically approaches its final self-similar profile (the thick curve with "$\infty$").

realistic cases. Below, we present a self-similar solution for the isothermal expansion of limited masses (Murakami et al., 2005). The solution explains plasma expansions under relatively long laser pulses or small-sized targets so that the solution responds to the above argument on target disintegration. Note that other self-similar solutions of isothermal plasma expansion have been found for laser-driven two-fluid expansions in light of ion acceleration physics (Murakami & Basko, 2006) and heavy-ion-driven cylindrical x-ray converter (Murakami et al., 1990), though they are not discussed here.

### 2.2 Isothermal expansion

The plasma is assumed to be composed of cold ions and electrons described by one temperature $T_e$, which is measured in units of energy as follows. Furthermore, the electrons are assumed to obey the Boltzmann statistics,

$$n_e = n_{ec} \exp(e\Phi/T_e) , \tag{15}$$

where $n_{ec}(t)$ is the temporal electron density at the target center, $e$ is the elementary charge, and $\Phi(r,t)$ is the electrostatic potential, the zero-point of which is set at the target center, i.e., $\Phi(0,t) = 0$. The potential $\Phi$ satisfies the Poisson equation,

$$\frac{1}{r^{\alpha-1}}\frac{\partial}{\partial r}\left(r^{\alpha-1}\frac{\partial \Phi}{\partial r}\right) = 4\pi e(n_e - Zn_i) , \tag{16}$$

where $Z$ is the ionization state; the superscript $\alpha$ stands for the applied geometry such that $\alpha$ = 1, 2, and 3 correspond to planar, cylinder, and spherical geometry, respectively. Throughout the present analysis, the electron temperature $T_e$ and the ionization state $Z$ are assumed to be constant in space and time.

An ion in the plasma is accelerated via the electrostatic potential in the form,

$$\frac{\partial v}{\partial t} + v\frac{\partial v}{\partial r} = -\frac{Ze}{m_i}\frac{\partial \Phi}{\partial r} , \tag{17}$$

where $m_i$ is the ion mass and $v$ is the ion velocity. Note that, in the following, we consider such a system that the plasma has quasi-neutrality, i.e., $n_e \approx Zn_i$, where $n_i$ and $n_e$ are the number densities of the ions and the electrons, respectively. Equations (15) and (17) are combined to derive a single-fluid description,

$$\frac{\partial v}{\partial t} + v\frac{\partial v}{\partial r} = -\frac{c_s^2}{\rho}\frac{\partial \rho}{\partial r} , \tag{18}$$

where $c_s = \sqrt{ZT_e/m_i}$ is the sound speed. Also, a fluid element with mass density $\rho(r,t) = m_i n_i$ satisfies the following mass conservation law,

$$\frac{\partial \rho}{\partial t} + \frac{1}{r^{\alpha-1}}\frac{\partial}{\partial r}(r^{\alpha-1}\rho v) = 0 . \tag{19}$$

We now seek a self-similar solution to Eqs. (18) and (19) on $\rho(r,t)$ and $v(r,t)$ under the similarity ansatz,

$$v = \dot{R}\xi \ , \ \ \xi \equiv \frac{r}{R}, \tag{20}$$

$$\rho = \rho_{00} \left(\frac{R}{R_0}\right)^{-\alpha} G(\xi), \tag{21}$$

where $R(t)$ stands for a time-dependent characteristic system size, and $\xi$ is the dimensionless similarity coordinate; the over-dot in Eq. (20) denotes the derivative with respect to time; $\rho_{00} \equiv \rho(0,0)$ and $R_0 \equiv R(0)$ are the initial central density and the size, respectively; $G(\xi)$ is a positive unknown function with the normalized boundary condition $G(0) = 1$. Then, Eqs. (15) and (21) give

$$n_e \approx n_{ec}(t)G(\xi) \approx Z\frac{\rho_{00}}{m_i} \left(\frac{R}{R_0}\right)^{-\alpha} G(\xi), \tag{22}$$

Under the similarity ansatz, Eqs. (20) and (21), the mass conservation, Eq. (19), is automatically satisfied. Substituting Eqs. (20) and (21) for Eq. (18), and making use of the derivative rules, $\partial/\partial r = R^{-1}\,(d/d\xi)$ and $\partial/\partial t = -\xi\dot{R}R^{-1}\,(d/d\xi)$, one obtains the following ordinary differential equations in the form of variable separation,

$$\frac{R\ddot{R}}{c_s^2} = -\frac{G'}{\xi G} = \psi_0 \ , \tag{23}$$

where $\psi_0 (> 0)$ is a separation constant, and the prime denotes the derivative with respect to $\xi$. Without losing generality, the constant $\psi_0$ can be set equal to an arbitrary numerical value, because this is always possible with a proper normalization of R and $\xi$. Here, just for simplicity, we set $\psi_0 = 2$ in Eq. (23). Then the spatial profile of the density, $G(\xi)$, is straightforwardly obtained under $G(0) = 1$ in the form (True et al., 1981; London & Rosen, 1986),

$$G(\xi) = \exp(-\xi^2) \, . \tag{24}$$

As was seen in Fig. 1, the density profile of isothermally expanding plasma with a limited mass is found to approach asymptotically the solution, Eq. (24), even if it has a different profile in the beginning. Meanwhile, $R(t)$ in Eq. (23) cannot be given explicitly as a function of time but has the following integrated forms,

$$\dot{R} = 2c_s\sqrt{\ln(R/R_0)} \, , \tag{25}$$

$$\frac{c_s t}{R_0} = \frac{1}{2}\int_1^{R/R_0} \frac{dx}{\sqrt{\ln x}} \ , \tag{26}$$

where in obtaining Eqs. (25) and (26), the system is assumed to be initially at rest, i.e., $\dot{R}(0) = 0$. Here it should be noted that Eqs. (23) - (26) do not explicitly include the geometrical index $\alpha$, and therefore they apply to any geometry.

Based on the solution given above, some other important quantities are derived as follows. First, the total mass of the system $M_0$ is conserved and given with the help of Eqs. (21) and (24) in the form,

$$M_0 = (4\pi)_\alpha \rho_{00} R_0^\alpha \int_0^\infty \xi^{\alpha-1} \exp(-\xi^2)\, d\xi = \left(\sqrt{\pi} R_0\right)^\alpha \rho_{00}\,, \tag{27}$$

with

$$(4\pi)_\alpha \equiv \begin{cases} 2, (\alpha = 1) \\ 2\pi, (\alpha = 2) \\ 4\pi, (\alpha = 3) \end{cases} = \frac{2\pi^{\alpha/2}}{\Gamma(\alpha/2)}\,, \tag{28}$$

where Γ is the Gamma function. Although the quantitative meaning of $R(t)$ was somewhat unclear when first introduced in Eq. (20), it can be now clearly understood by relating it to the temporal central density, $\rho_c(t) \equiv \rho(0,t) \approx m_i n_{ec}(t)/Z$, with the help of Eqs. (21) and (27) in the form,

$$R(t) = \frac{1}{\sqrt{\pi}} \left(\frac{M_0}{\rho_c(t)}\right)^{1/\alpha}. \tag{29}$$

Additionally the potential Φ and corresponding electrostatic field $E = -\nabla\Phi$ are obtained from Eqs. (15), (21), (22), and (24) in the following forms,

$$\frac{e\Phi}{T_e} = -\xi^2\,, \tag{30}$$

$$\frac{eE}{T_e} = \frac{2\xi}{R}\,. \tag{31}$$

The above field quantities contrast well with the fields of the SP solution obtained for a semi-infinitely stretched planar plasma: $e\Phi/T_e = -1 - x/c_s t$ and $eE/T_e = 1/c_s t$ for $x/c_s t \geq -1$ and $t > 0$. It is here worth emphasizing that the electrostatic field increases linearly with $\xi$ for the present model, while it is constant in space for the SP model. Furthermore, the kinetic energy of the system $E_k(t)$ is given with the help of Eqs. (20), (21) and (27) by

$$E_k = \frac{(4\pi)_\alpha}{2} \rho_{00} R_0^\alpha \dot{R}^2 \int_0^\infty \xi^{\alpha+1} \exp(-\xi^2)\, d\xi = \frac{\alpha}{4} M_0 \dot{R}^2, \tag{32}$$

while the internal (thermal) energy of the system $E_i(t)$ is kept constant,

$$E_i = \frac{3 M_0 Z T_e}{2 m_i} = \frac{3}{2} M_0 c_s^2\,. \tag{33}$$

Correspondingly, the power required to keep the isothermal expansion, $P(t) = dE_k/dt$, is given from Eqs. (23), (25), and (32) in the form,

$$P/P_0 = \sqrt{\ln(R/R_0)}\,/(R/R_0\,), \tag{34}$$

where $P_0 = 2\alpha M_0 c_s^3/R_0$.

The ion energy spectrum is a physical quantity of high interest. In the present model, the kinetic energy of an ion in flight directly relates its location, in other words, the further an

ion is located, the faster it flies. Then, the number of ions contained in an infinitesimally narrow area of the similarity coordinate between $\xi$ and $\xi + d\xi$ is given by

$$dN = (4\pi)_\alpha n_{i00} R_0^\alpha \xi^{\alpha-1} \exp(-\xi^2)\, d\xi \,, \tag{35}$$

where $n_{i00} = \rho_{00}/m_i$ is the initial number density of the ions at the center. Meanwhile, the kinetic energy of an ion at $\xi$ is $\varepsilon = m_i \dot{R}^2 \xi^2/2$, and therefore

$$d\varepsilon = m_i \dot{R}^2 \xi d\xi \,. \tag{36}$$

From Eqs. (35) and (36), the ion energy spectrum is obtained,

$$\frac{d\widehat{N}}{d\hat{\varepsilon}} = \frac{\hat{\varepsilon}^{(\alpha-2)/2} \exp(-\hat{\varepsilon})}{\Gamma(\alpha/2)}, \tag{37}$$

where $\widehat{N} \equiv N/N_0$ and $\hat{\varepsilon} \equiv \varepsilon/\varepsilon_0$ are normalized quantities with

$$\varepsilon_0(t) = m_i \dot{R}^2/2 \,, \tag{38}$$

$$N_0 = (\sqrt{\pi} R_0)^\alpha n_{i00} \,. \tag{39}$$

It should be noted that, for $\alpha$ = 3, the energy spectrum, Eq. (37), coincides with the well-known Maxwellian energy distribution; this is not just a coincidence because an isotropically heated mass always has such a distribution.

Although the spectrum, Eq. (37), is for the ion number density, another spectrum for the energy density, $dE_k/d\varepsilon$, is an even more interesting quantity. It can be easily obtained quite in the same manner as for $dN/d\varepsilon$ taking the specific kinetic energy $v^2/2$ into account:

$$\frac{dE_k}{d\hat{\varepsilon}} = \frac{\varepsilon_0 N_0}{\Gamma(\alpha/2)} \hat{\varepsilon}^{\alpha/2} \exp(-\hat{\varepsilon}) \,. \tag{40}$$

The peak value of Eq. (40) is attained at $\hat{\varepsilon} = \alpha/2$, which is three times higher than that of Eq. (37) for the spherical case ($\alpha = 3$).

### 2.3 Comparison with experiments

We apply the analytical model to two different laser experiments focusing on the ion energy spectrum. The two experimental results were separately obtained under different conditions by means of the time-of-flight method. In both cases, the laser conditions were almost the same, i.e., the wavelength $\lambda_L = 1.06\,\mu m$, the irradiation intensity $I_L = 0.5 - 1.0 \times 10^{11}\, W/cm^2$, and the pulse length $\tau_L \sim 10\, ns$ with a sufficiently large F-number of a focal lens. Moreover, the target thicknesses were $R_0 \sim 10\, \mu m$. Once the key laser parameters, $I_L$ and $\tau_L$, are given, the other basic parameters required for the model analysis are calculated. For example, the plasma temperature is roughly estimated from the power balance, $\eta_a I_L \approx 4\rho_{cr} c_s^3$ (Murakami & Meyer-ter-Vhen, 1991), where $\eta_a$ is the absorption efficiency and $\rho_{cr}$ is the critical mass density:

$$T_e\ [eV] = 27(A/Z)^{1/3} \hat{\lambda}_L^{4/3} \left(\eta_a \hat{I}_L\right)^{2/3}, \tag{41}$$

where $A$ is the ion mass number. The corresponding sound speed turns out to be in the order of $10^6 cm/s$, and the disintegration time $\sim 2R_0/c_s$ (recall Fig. 1) is calculated to be

about 1 ns ($\ll \tau_L \sim 10\ ns$). The normalized radius $R/R_0$ at the laser turn-off is obtained by Eq. (26) as a function of the normalized time $\tau_L/(R_0/c_s)$. In addition, the scale length of the plasma expansion is $c_s\tau_L \sim 100\ \mu m (\gg R_0 \sim 10\ \mu m)$. Therefore, the present self-similar analysis is considered to be applicable to the experiments under consideration. From the above key numerical values, the characteristic ion kinetic energy at the laser turn-off defined by Eq. (38) is roughly estimated to be $\varepsilon_0 = 2.5 - 3.5$ keV.

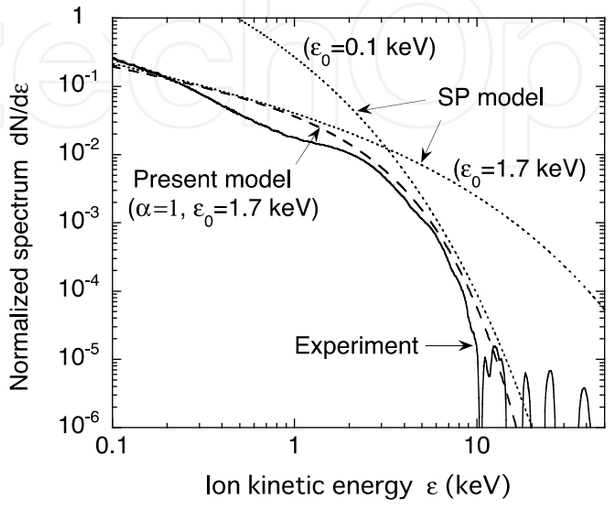


Fig. 2. Comparison of the experimental result (solid line) and the analytical curve (dashed line) obtained by Eq. (37) under planar geometry. Dotted curves for reference are obtained by the SP model, Eq. (42).

In the first case, a laser beam was irradiated on a spherical target with diameter of 500 $\mu m$, which was composed of 8$\mu m$-thick plastic shell coated by a 100 nm-thick tin (Sn) layer. In this case, the plasma expansion during the laser irradiation can be regarded as quasi-planar, because the plasma scale ~100 $\mu m$ is appreciably smaller than the laser spot size ~500 $\mu m$. As mentioned in the introduction, the purpose of the Sn-coat was to observe the characteristics of the EUV light and energetic ion fluxes emitted from the Sn plasma. The detector was tuned to observe massive Sn ions in the direction of 30 degrees with respect to the beam axis. Figure 2 shows the ion energy spectrum comparing the experimental result (solid line) and the analytical curve (dashed line) obtained by Eq. (37) with a fitted numerical factor $\varepsilon_0 = 1.7$ keV and $\alpha = 1$ (planar geometry). With respect to the vertical axis, the physical quantities are properly normalized such that the peak values stay in the order of unity. The fluctuated structure of the experimental data for $\varepsilon > 10$ keV cannot be clearly judged as concerns whether the signals simply span the region with less precision of diagnosis, or whether they should be attributed to other causes such as carbon ions, protons, and photons. In Fig. 2, two other curves (dotted lines) are also plotted for comparison. They are obtained by the SP model (Mora, 2003),

$$\frac{dN}{d\hat{\varepsilon}} \propto \frac{\exp\left(-\sqrt{\hat{\varepsilon}}\right)}{\sqrt{\hat{\varepsilon}}}, \tag{42}$$

where $\varepsilon_0 = 1.7$ keV and $\varepsilon_0 = 0.1$ keV are used to draw the fitted curves to relatively low and high energy regions, respectively. It can be seen that it is hard to reproduce the experimental

result by Eq. (42). The essential difference of the two analytical models is attributed to their density profiles, i.e., $\rho \propto \exp(-\xi^2)$ for the present model and $\rho \propto \exp(-\xi)$ for the SP model. This can be elaborated on as follows: The pressure scale decreases with time all over the region in the present model, while it is kept constant in time in the SP model. Therefore, the ions in the former model are less accelerated due to the pdV work than those in the latter model.

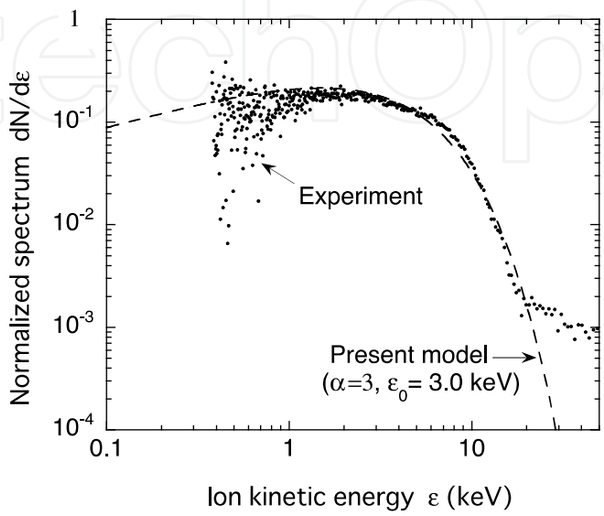


Fig. 3. Comparison of the experimental result (dots) and the analytical curve (dashed line) obtained by Eq. (37) under spherical geometry.

In the second case, a laser beam was irradiated from a single side with a liquid-Xe jet ejected through a nozzle with diameter of 30 $\mu m$. The focal spot size was also 30 $\mu m$ in diameter. Therefore, the resultant plasma expansion was very likely unsymmetrical. In this case, however, the specific mass can expand into much larger space three-dimensionally than in the first case, and thus is regarded as a quasi-spherical expansion ($\alpha = 3$). Figure 3 shows the experimental result and an analytical curve obtained by Eq. (37) with a fitted numerical factor $\varepsilon_0 = 3.0$ keV. Again, with respect to the vertical axis, the physical quantities are properly normalized such that the peak values stay in the order of unity. The ion fluxes were observed at an angle of 45 degrees with respect to the laser beam axis. The experimental signals strongly fluctuate at energies close to the lowest detection limit at around $\varepsilon \sim 400$ eV, but are otherwise well reproduced by the analytical curve.

## 3. Laser-driven nonstationary accelerating foil due to nonlinear heat conduction

### 3.1 Introduction

When one side of a thin planar foil is heated by an external heat source, typically by laser or thermal x-ray radiation, the heated material quickly expands into vacuum with its density being reduced drastically - this phenomenon is called "ablation". In inertial confinement fusion (ICF) research, for example, it is indispensable to correctly understand the shell acceleration due to ablation. Thereby self-similar solutions play a crucial role in the analysis and prediction of the detailed behavior of the shell acceleration. Although some analytical

models have been proposed to study the shell acceleration due to mass ablation (Gitomer et al., 1977; Takabe et al., 1983; Kull, 1989, 1991), most of them have assumed a stationary ablation layer. Pakula and Sigel (1985), for example, reported a self-similar solution for the ablative heat wave. In the solution, however, the ablation surface is ideally treated such that the density goes to infinity, and the surface does not accelerate. Below, we present a new self-similar solution (Murakami et al, 2007), which describes non-stationary acceleration dynamics of a planar foil target ablatively driven by non-linear heat transfer. The most striking differences from the other models are that the target has a decreasing mass with a peak density, and that it has a distinct shell/vacuum boundary, where the density and the temperature converge to null.

### 3.2 Basic equations and similarity ansatz

Suppose that a planar shell is being accelerated in the positive direction of the $x$-axis in an inertial laboratory frame via the recoil force due to the ablation. The characteristic scale length of the shell $D(t)$ decreases with time. Let us assume that the shell is burnt out at the origin of the coordinates, i.e., $D(0) = 0$ at $x = 0$. One can always find such an inertial frame by appropriately choosing relative position and velocity to another reference inertial frame. In this case the shell velocity is initially ($t < 0$) negative, its absolute value gradually decreases due to the positive acceleration, and finally the burned-out shell halts at $(x, t) = (0,0)$. The fluid system is then described by the following equations:

$$\frac{\partial \rho}{\partial t} + \frac{\partial (\rho v)}{\partial x} = 0 \,, \tag{43}$$

$$\frac{\partial v}{\partial t} + v\frac{\partial v}{\partial x} = -\frac{\partial p}{\partial x}, \tag{44}$$

$$\rho\left(\frac{\partial \epsilon}{\partial t} + v\frac{\partial \epsilon}{\partial x}\right) + p\frac{\partial v}{\partial x} = \frac{\partial}{\partial x}\left(\kappa\frac{\partial T}{\partial x}\right), \tag{45}$$

where $\rho$ is the mass density, $v$ is the flow velocity, $\epsilon$ is the specific internal energy, $T$ is the temperature in units of energy, and $\kappa$ is the thermal conductivity. We assume an ideal gas equation of state in the form,

$$p = \rho T, \ \epsilon = T/(\gamma - 1), \tag{46}$$

where $\gamma$ is the specific heats ratio. We assume that the thermal conductivity is expressed in the following power-law form with $m$, $n$, and $\kappa_0$ being constants,

$$\kappa = \kappa_0 T^n/\rho^m. \tag{47}$$

We introduce the following well-known similarity ansatz (Guderley, 1942; Lie, 1970) to eliminate the temporal dependence of the system and thus to find a self-similar solution:

$$\eta = x/D(t) \,, \ D(t) = A(-t)^\alpha \,, \ \alpha \geq 1 \,, \tag{48}$$

$$v = \alpha A(-t)^{\alpha-1} u(\eta) \,, \tag{49}$$

$$T = (\alpha A)^2(-t)^{2(\alpha-1)}\theta(\eta)\,, \tag{50}$$

$$\rho = B(-t)^{\beta} g(\eta)\,, \qquad \beta = \frac{2(n-1)(\alpha-1)-1}{1+m}\,, \tag{51}$$

where $\eta$ is the self-similar variable; $u(\eta)$, $\theta(\eta)$, and $g(\eta)$ stand for the self-similar profiles of the velocity, temperature, and density, respectively; $\alpha$, $A$ and $B$ are arbitrary constants. In most of numerical calculations in this paper, we employ $\alpha = 2$ (constant acceleration), $(m,n) = (0,5/2)$ (electron heat conductivity) and $\gamma = 5/3$ as a reference case. The constraint, $\alpha \geq 1$, in Eq. (48) stems from Eqs. (49) and (50) in order that $v$ and $T$ do not diverge to infinity as $t \to 0$. The limiting value, $\alpha = 1$, corresponds to a special case, where the characteristic scale of $v$ and $T$ are kept constant in time, while $\alpha = (2n-1)/2(n-1) = 4/3$ corresponds to another special case, where the density scale does not change in time, i.e., $\beta = 0$ [see Eq. (51)].

Using ansatz (48) - (51), Eqs. (43) - (45) are reduced to the following set of ordinary differential equations:

$$(u+\eta)g' + \left(u' - \frac{\beta}{\alpha}\right)g = 0\,, \tag{52}$$

$$(u+\eta)\,u' + (\alpha^{-1}-1)u + (g\theta)'/g = 0\,, \tag{53}$$

$$(\gamma-1)^{-1}[(u+\eta)\,\theta' + 2(\alpha^{-1}-1)\theta] + \theta u' = Kg^{-1}(g^{-m}\theta^n\theta')' \tag{54}$$

where the prime denotes the derivative with respect to $\eta$, and

$$K = \kappa_0 \alpha^{2n-1} A^{2n-2} B^{-1-m} \tag{55}$$

is a dimensionless parameter. Solving Eqs. (52) and (53) algebraically for $g'$ and $u'$, one finds that a singular point appears when $u + \eta = \pm\sqrt{\theta}$ (more details on the singular point will be given later). Let $\eta_s$, $u_s$, $g_s$, and $\theta_s$ be their values at the singular point. Here we introduce re-normalized variables, ξ, U(ξ), G(ξ), and Θ(ξ):

$$\xi = \frac{\eta-\eta_s}{\sqrt{\theta_s}}\,, \qquad \xi = \frac{u-\eta_s}{\sqrt{\theta_s}}\,, \qquad G = \frac{g}{g_s}\,, \qquad \Theta = \frac{\theta}{\theta_s}\,, \tag{56}$$

At the singular point, $\xi = 0$, the re-normalized variables are specified to be

$$U(0) = -1, \quad G(0) = 1, \quad \Theta(0) = 1, \tag{57}$$

where we employ the flow direction such that $u_s + \eta_s = -\sqrt{\theta_s}$. Equations (10) - (12) are then transformed to

$$(U+\xi)\,G' + (U' - \beta/\alpha)G = 0\,, \tag{58}$$

$$(U+\xi)\,U' + (\alpha^{-1}-1)U + (G\Theta)'/G + K_1 = 0\,, \tag{59}$$

$$(\gamma-1)^{-1}[(U+\xi)\,\Theta' + 2(\alpha^{-1}-1)\Theta] + \Theta U' = K_2 G^{-1}(G^{-m}\Theta^n\Theta')' \tag{60}$$

where the prime hereafter denotes the derivative with respect to $\xi$, and

$$K_1 = (1-\alpha^{-1})\eta_s/\sqrt{\theta_s}\,,\ K_2 = K\theta_s^{n-1}g_s^{-m-1}\,, \tag{61}$$

are dimensionless constants representing the gravity (acceleration) and the heat conductivity, respectively. Thus the system is clearly defined by Eqs. (57) - (60). Equations (58) and (59) yield

$$G' = \frac{\Delta_2}{\Delta_1}G\,, \qquad U' = \frac{\beta}{\alpha} - (U+\xi)\frac{\Delta_2}{\Delta_1}, \tag{62}$$

where

$$\Delta_1 = (U+\xi)^2 - \Theta\,, \tag{63}$$

$$\Delta_2 = \left(\frac{\beta}{\alpha}\right)(U+\xi) + (\alpha^{-1}-1)U + \Theta' + K_1\ . \tag{64}$$

It is clear that G′ and U′ in Eq. (62) are singular when $\Delta_1 = 0$. This singular point corresponds to the sonic point, where the flow velocity relative to the surface $\xi = const$ is equal to the local isothermal sound speed. An integrated curve which is physically acceptable is expected to pass this singular sonic point smoothly, the condition of which is given by

$$\Delta_1 = \Delta_2 = 0\,. \tag{65}$$

Since $\xi = 0$ is the singular point, one should start numerical integration at its infinitesimally adjacent point. One then needs the four derivatives $G'(0)$, $U'(0)$, $\Theta'(0)$, and $\Theta''(0)$, which are fully provided by relation (65). At $\xi = 0$, the derivatives of Eq. (62) are reduced from L'Hopital's theorem to

$$G' = \frac{\Delta_2'}{\Delta_1'}\,, \quad U' = \frac{\beta}{\alpha} + \frac{\Delta_2'}{\Delta_1'}\,. \tag{66}$$

Thus all the four derivatives at the sonic point are explicitly obtained from Eqs. (57) - (60), and (66).

The present system has another singular point at the vacuum interface, the coordinate at which, $\xi = \xi_v$, is an eigenvalue of the system. On the vacuum interface the relative flow velocity to the free surface vanishes, i.e., $U(\xi_v) + \xi_v = 0$, which can also be interpreted as the definition of the free surface. Moreover at $\xi = \xi_v$ the pressure and thus the density are expected to vanish coherently, because practically no heat conduction prevails in this front region (typically characterized such that $G \gg 1$, $\Theta \ll 1$, and $(U+\xi)^2 \ll \Theta$) and thus the specific entropy is kept constant in time. It is then shown that Eqs. (16) and (18) (neglecting the heat conduction) have the adiabatic integral with an arbitrary constant $c_0$ (Zel'dovich & Raizer, 1966):

$$\Theta(U+\xi)^{\mu}G^{\mu+1-\gamma} = c_0, \qquad \mu \equiv \frac{2(1-\alpha)+\beta(\gamma-1)}{\alpha+\beta}. \tag{67}$$

The vacuum interface is a singular point of the adiabatic flow of the saddle type (Sanz et al., 1988), where the spatial profiles in the vicinity of $\xi = \xi_v$ is worked out from Eqs. (58) - (60) to a first-order approximation in $(\xi_v - \xi)$:

$$\Theta \approx \frac{\big((\gamma+1)\alpha-2\big)(\alpha K_1+(\alpha-1)\xi_v)}{(\alpha+\beta)\gamma}(\xi_v-\xi), \tag{68}$$

$$U+\xi \approx -\frac{\gamma+1-2\alpha^{-1}}{\gamma}(\xi_v-\xi) \tag{69}$$

$$G \approx c_1(\xi_v-\xi)^{\nu}, \quad \nu \equiv \frac{-\alpha+\beta\gamma+2}{\alpha(\gamma+1)-2}, \tag{70}$$

where $c_1$ is an arbitrary constant; $c_1 \approx G_a(\xi_v-\xi_a)^{-\nu}$ for a relatively high aspect shell, i.e., $G_a/(\xi_v-\xi_a) \gg 1$, where $G_a$ and $\xi_a$ are their corresponding values at the density peak; $G_a$ and $\xi_a$ are also eigenvalues of the system as will be given below together with $\xi_v$. In particular, under constant acceleration ($\alpha = 2$), the velocity becomes constant, $U = -\xi_v$, and $G \propto (\xi_v-\xi_a)$ apart from a linear temperature profile in space, as one can predict from Eqs. (69) and (70).

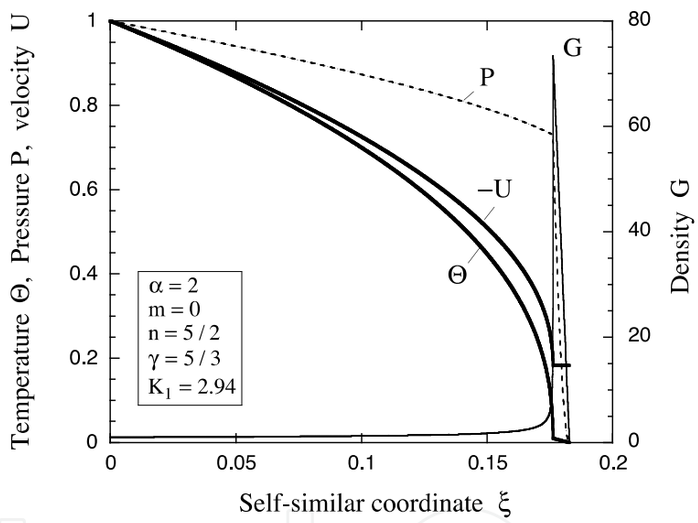


Fig. 4. Eigenstructure of the accelerated shell under a constant gravity ($\alpha = 2$).

### 3.3 Two dimensional eigenvalue problem and numerical results

Although one can start the numerical integration at $\xi = 0$ toward the positive direction of $\xi$-axis, it soon turns out that such numerical integrations produce physically unacceptable pictures under an arbitrary set of the values of $K_1$ and $K_2$ such that $G \to \infty$ on its way in the integration without showing the converging behavior, Eqs. (68) - (70), at the vacuum boundary. Therefore the present system is supposed to be an eigenvalue problem, in which only some special combinations of $K_1$ and $K_2$ can produce the converging behavior expected as a physically meaningful solution (Murakami et al., 2004).

Figure 4 shows such an eigenstructure numerically obtained for the density $G$, the temperature $\Theta$, the velocity $U$, and the pressure $P = G\Theta$ under the fixed parameters given in Fig. 4. As mentioned earlier, the spatial profiles thus obtained strikingly contrast with ones for the stationary ablation models (Gitomer et al., 1977; Takabe et al., 1983; Kull, 1989, 1991).

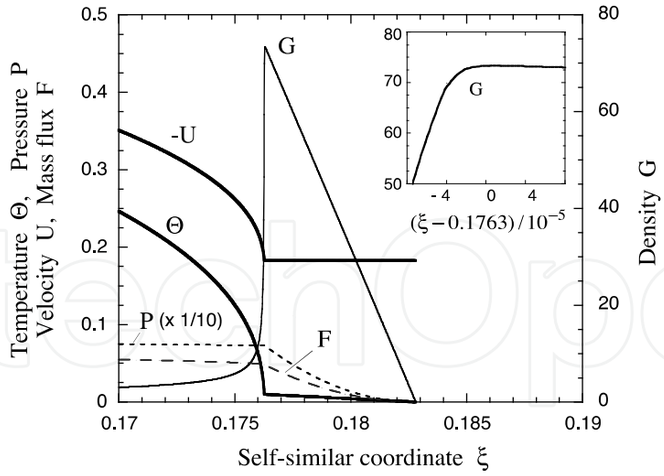


Fig. 5. Magnified view of Fig.4 around the ablation surface.

Figure 5 shows the magnified view around the ablation surface of Fig. 4, in which the mass flux relative to the surface with $\xi = const$, $F \equiv -(U+\xi)G$, is additionally depicted. Surprisingly the predicted profiles, (68) - (70), apply not only to the vicinity of the vacuum boundary but also to almost all the region beyond the ablation surface ($\xi > 0.1763$). This in turn supports the earlier argument that the heat conduction in the shell is practically negligible. It should also be noted that at $\xi = \xi_a$ the physical quantities seemingly have a sharp jump in their derivatives. However, all those quantities change smoothly but on a very narrow range, which can be observed in the further magnified view for $G$ in the upper right corner in Fig. 5. The characteristic scale length of the drastic change in the physical quantities can be roughly estimated from Eq. (60) to be $\Delta\xi_a \sim \Theta_a^n/|U_a|\, G_a^{1+m} \sim \mathcal{O}(10^{-5})$ as can be observed in Fig. 5.

## 4. Gravitational collapse of radiatively cooling sphere in view of star-formation

### 4.1 Introduction

Self-similar solutions play a crucial role in astrophysics as well. Below we describe a spherically contracting system observed in the star formation processes, in which the effect of radiative heart conduction is expected to play an important role. In such a system, substantial dissociation and ionization of molecules and atoms proceed with time, and the isothermal assumption used in the so-called LP model (Larson, 1969; Penston, 1969) becomes inappropriate. A solution introduced here (Murakami et al., 2004) can be clearly placed in a thermodynamic perspective as follows: The LP model with the isothermal assumption means infinitely large heat conductivity, i.e., $Pe \to 0$, where $Pe$ denotes the Péclet number. Meanwhile, there are a number of works based on the perfect adiabaticity, i.e., $Pe \to \infty$, which corresponds to zero heat conductivity (Sedov, 1959; Barenblatt, 1979; Antonova, 2000). These are two opposed limiting cases, with which the analytical and numerical treatment are substantially simplified, and the energy conservation law is often expressed in an integrated form or neatly installed in the equation of motion. In contrast, we explicitly leave the radiative conduction term in the hydrodynamic system to handle its nonlinear effect.

An important feature of the present subsection, which is essentially different from the conventional ones obtained under the isothermal or adiabatic assumptions, is that all the scales of the physical quantities are uniquely determined as a function of time only. This is clear from the following argument: When discussing self-similarity within the one-dimensional framework, one needs four physical quantities to produce a dimensionless parameter as a basic self-similar variable, where the system is contained in the class of systems of the so-called MLT fundamental units of measurement. Radius $r$, time $t$, and the gravitational constant $G$, are apparently the first three quantities in a spherically contracting system under self-gravity. The fourth quantity is, for example, the temperature for an isothermal system, or the specific entropy for an adiabatic system. Such quantities cannot be specified in the absolute value, and therefore they can serve as an external control parameter of individual systems. In the present system, however, the fourth quantity is the heat diffusion conductivity, $\nu_0$; the numerical value of which is quite unique, once the conductive mechanism is specified. Therefore $\nu_0$ can never be a control parameter, and the resultant behavior of the system is unique.

### 4.2 Basic equation and similarity ansatz

The one-dimensional spherical gas-dynamical equations with both self-gravity and diffusivity are

$$\frac{\partial \rho}{\partial t} + \frac{1}{r^2}\frac{\partial}{\partial r}(r^2 \rho u) = 0, \tag{71}$$

$$\frac{\partial u}{\partial t} + u\frac{\partial u}{\partial r} = -\frac{1}{\rho}\frac{\partial p}{\partial r} - \frac{\partial \phi}{\partial r}, \tag{72}$$

$$\frac{1}{r^2}\frac{\partial}{\partial r}\left(r^2 \frac{\partial \phi}{\partial r}\right) = 4\pi G\rho, \tag{73}$$

$$\rho\left(\frac{\partial \epsilon}{\partial t} + u\frac{\partial \epsilon}{\partial r}\right) + \frac{p}{r^2}\frac{\partial}{\partial r}(r^2 u) = \frac{1}{r^2}\frac{\partial}{\partial r}\left(r^2 \nu \frac{\partial T}{\partial r}\right) \tag{74}$$

where $p$ is the pressure, $\rho$ the density, $\epsilon$ the specific internal energy, $u$ the flow velocity, and $\phi$ the gravitational potential. We assume the ideal gas equation of state (EOS) in the form,

$$\frac{(Z+1)k_B}{\mu}T = \frac{p}{\rho} = (\gamma - 1)\epsilon, \tag{75}$$

where $k_B$ is the Boltzmann constant, $\mu$ the mean atomic mass, and $\gamma$ the specific heats ratio; $Z$ is the ionization state, and $Z = 1$ is assumed for hydrogen plasma. Equation (74), described by the one-temperature model, includes the non-linear heat diffusion term on the right hand side, where we assume a power-law dependence for the diffusion coefficient, $\nu = \nu_0 T^n/\rho^m$, with $\nu_0$, $m$, and $n$ being constants. For normal physical values, $n > 0$ and $m > 0$ are assumed. With an intention to apply our solution primarily to the case of radiative heat diffusion, we can express $\nu$ as $\nu = (16\sigma_{SB}\, T^3)/3\kappa_R$ where $\kappa_R = \kappa_0 \rho^m / T^{n-3}$ is the Rosseland

mean opacity, $\sigma_{SB}$ is the Stefan-Boltzmann constant, and $\kappa_0 = 16\sigma_{SB}/3\nu_0$ is a constant. In the formulae given below, we keep the generality in terms of the parameters, $m$, $n$, and $\gamma$, but also show specific forms using the values of the reference set at the same time: $m = 2$, $n = 13/2$, and $\nu_0$ describing the opacity due to inverse bremsstrahlung in a fully ionized hydrogen plasma (Zel'dovich & Raizer, 1966) together with $\gamma = 5/3$.
To find a self-similar solution, we here introduce the following group transformation,

$$r = \lambda\hat{r}, \quad t = \lambda^a\hat{t}, u = \lambda^b\hat{u}, T = \lambda^c\hat{T}, \rho = \lambda^d\hat{\rho}, \phi = \lambda^e\hat{\phi} \tag{76}$$

where the hats denote the physical quantities in the scaled system related by the scale factor $\lambda$ with the parent system without hats. The constants, *a, b, c, d*, and *e*, can be appropriately determined by substituting Eq. (76) for Eqs. (71) - (74) such that the transformed system is kept symmetric and thus has the same structure as the original one based on the Lie's idea (Lie, 1970):

$$1 - a = b = c/2 = 1 + d/2 = e/2 = (1 * 2m)/(3 + 2m - 2n). \tag{77}$$

For the reference case, $m$ = 2 and $n$ = 13/2, Eq. (77) gives $a = 11/6$, $b = -5/6$, $c = e = -5/3$, and $d = -11/3$. Equation (77), together with the following similarity ansatz, enables the removal of the temporal dependence from Eqs. (71) - (74),

$$R(t) = A\,|t|^{1/a}, \ \xi \equiv \mathrm{r/R(t)}, \tag{78}$$

$$u = \frac{A}{a}|t|^{b/a}v(\xi), \tag{79}$$

$$T = \left(\frac{A}{a}\right)^2 |t|^{c/a}\tau(\xi), \tag{80}$$

$$\rho = B|t|^{-2}g(\xi), \tag{81}$$

$$\frac{\partial\phi}{\partial r} = \frac{ABG}{\xi^2}|t|^{(c-1)/a}\Omega(\xi), \qquad \Omega(\xi) \equiv 4\pi\int_0^\xi g(\xi)d\xi, \tag{82}$$

where $R(t)$ is the temporal characteristic scale length of the system; $A$ and $B$ are positive constants defining the scales of the radius and the density, respectively. Note that the relation, $d/a = -2$, is used for the similarity ansatz of the density in Eq. (84), which holds regardless of the values of $m$ and $n$. Furthermore, it should be noted that, at a glance, the ansatz for $u$ and $T$ given in Eqs. (82) and (83) seem to be bounded with each other with the similar front factors, $A/a$ and $(A/a)^2$, respectively. However, these factors are chosen just for simplicity, and $u$ and $T$ are kept independent of each other, because the functions, $v(\xi)$ and $\tau(\xi)$, are left free until they are self-consistently determined as the solution of the eigenvalue problem as shown below. In this paper, we consider a contracting fluid system for $t < 0$ which collapses at $t = 0$, and therefore $|t| = -t$. Then, Eqs. (71), (72), and (74) are respectively reduced to the following ordinary differential equations,

$$-(\pm\xi - v)g' + \left(\pm d + v' + \frac{2v}{\xi}\right)g = 0, \tag{83}$$

$$\pm bv - (\pm\xi - v)v' + \frac{(g\tau)'}{g} + \frac{K_1\,\Omega}{\xi^2} = 0, \tag{84}$$

$$\frac{\pm c\tau - (\pm\xi - v)\tau'}{\gamma - 1} + \left(v' + \frac{2v}{\xi}\right)\tau = K_2\frac{(\xi^2 g^{-m}\tau^n\tau')'}{g\xi^2}, \tag{85}$$

where the prime denotes the derivative with respect to $\xi$, and concerning the double signs, $(\pm)$, the upper (plus) and lower (minus) sign correspond to $t > 0$ and $t < 0$, respectively. Since Eq. (73) is automatically satisfied, its reduced form does not appear in the above set of equations. Thus, the present system is characterized by the two positive dimensionless parameters, $K_1$ and $K_2$, defined by $K_1 = a^2GB$ and $K_2 = (v_0/aB^{m+1})(A/a)^{2n-2}$. It can be interpreted that $K_1$ and $K_2$ are introduced for simplicity instead of $A$ and $B$. Equations (83) - (85) are second-order ordinary equation system for $g$, $\tau$, and $v$, and the obvious boundary conditions are

$$v(0) = 0,\ g(0) = 1,\ \tau(0) = 1,\ (g\tau)'_{\xi=0} = 0. \tag{86}$$

The last relation means that there is no pressure gradient at the center.

### 4.3 The self-similar solution as two dimensional eigenvalue problem

At first glance, the ODE system, Eqs. (83) - (85), together with the boundary condition (86), seem to be closed mathematically. However, one can easily find that numerical integration of the system produces a physically unacceptable picture under an arbitrary set of the values for $K_1$ and $K_2$ such that the temperature suddenly diverges to infinity at a finite radius. Since the physical quantities are expected to change smoothly in space, it is conjectured that some special values of $K_1$ and $K_2$, which are still unknown, can give such a physically acceptable picture. Therefore the present system is supposed to be a two-dimensional eigenvalue problem, which is essentially different from the one-dimensional eigenvalue problems of the previous work.

To determine a unique set of parameters, $K_1$ and $K_2$, we need two more physical conditions. The first one is quite an orthodox prescription, in which the right integration curve smoothly passes through the singular point, which is located somewhere at a finite distance from the center. On this singular point, the fluid velocity is equal to the local sound speed. The second parameter is less obvious compared with the first one, but still seems natural enough, namely, that both the density and the temperature converge to zero simultaneously with an increase in radius. The numerical calculation is started from the center, and therefore it is necessary to make clear the asymptotic behavior of the solution in the vicinity of the center as follows.

For the central region, the asymptotic behaviors of the above physical quantities are obtained by inserting the following ansatz,

$$g = 1 - g_0\xi^2,\ \tau = 1 - \tau_0\xi^2,\ v = -v_0\xi,\ (\xi \ll 1), \tag{87}$$

into Eqs. (83) - (85), where $g_0$, $\tau_0$, and $v_0$ are unknown positive constants, where we make use of the symmetry at the center and thus employed only the lowest quadratic terms for $g$ and $\tau$. After some manipulation, the constants are obtained,

$$v_0 = \frac{2(n-1)}{3(n-m-3/2)} \ , \tau_0 = \frac{(\gamma-1)n-m-\gamma+1/2}{3(\gamma-1)(n-m-3/2)K_2} g_0 = 2\pi K_1 - \frac{\tau_0 v_0^2}{4} \tag{88}$$

As can be seen in Eq. (88), in order to conduct the numerical calculation starting from the center, $K_1$ and $K_2$ must both be specified as trial values, which are expected to converge to their genuine eigenvalues after numerical iteration. Figure 6 shows the first step of the solving process, or how a right eigenvalue, $K_2$, is obtained on the $g$-$\tau$ plane, where $K_1 = 0.64$ is fixed just as a trial value. As can be seen in Figure 6, there exists an appropriate value of $K_2$, with which the integrated curve smoothly passes through the singular point, while the other integrated curves deviate from the right curve as the integration proceeds toward the singular point, resulting in an unacceptable physical picture. In this manner, an appropriate eigenvalue $K_2$ can be determined as a function of arbitrary $K_1$.

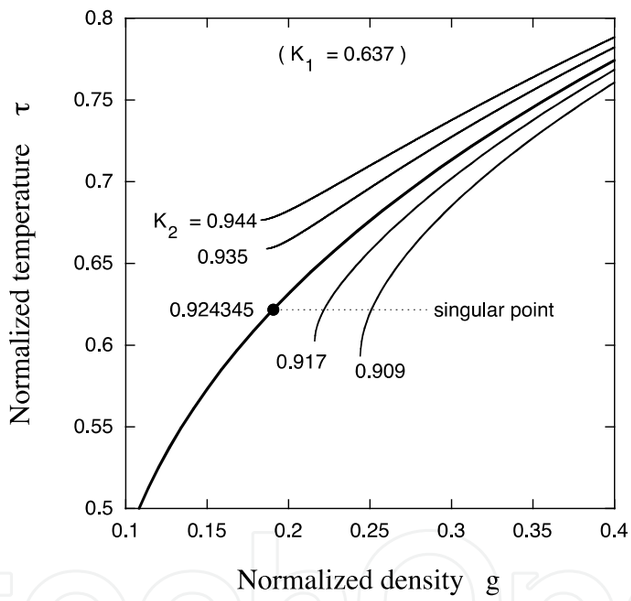


Fig. 6. g - $\tau$ diagram showing the optimization process of the eigenvalue, $K_2$.

Under the condition that the right integrated curve is to smoothly pass through a singular point, the integrations are conducted from the center ($g = \tau = 1$) with the radius toward infinity corresponding to $g = \tau = 0$. Fixed parameters are $m = 2$, $n = 13/2$, $\gamma = 5/3$, and $K_1 = 0.64$. As the second step, one needs to determine $K_1$ that satisfies the second requirement mentioned earlier, namely, $g \to 0$ and $\tau \to 0$ at the same time. Figure 7 shows how the right eigenvalue, $K_1$, is determined on the $g$-$\tau$ plane, where each curve is already optimized such that it passes through each singular point. As a result, it turns out that there exists a unique pair of the eigenvalues of $K_1$ and $K_2$, which satisfies the both requirements.
Figure 8 shows the eigenstructure for the temperature, $\tau \propto T$ the density, $g \propto \rho$, the velocity, $v \propto u$, and the heat flux, $\boldsymbol{q} \propto -v\nabla T$, under the eigenvalues of the reference system thus obtained, where the curves are assigned with labels corresponding to the original physical

quantities just for readers' comprehension. The behavior of the velocity for $v \to \infty$ may seem physically unacceptable at least in a rigorous sense. As a matter of fact, however, there are a number of examples for implosions and explosions in which the velocity profile is approximately linear with the radius (Sedov, 1959; Bernstein, 1978). In addition, the physical condition at enough large radii ($\xi \gg 1$) will not affect the core dynamics for an intermediate time period. Therefore, when we restrict our considerations to a finite closed volume containing the core, the present self-similar solution is expected to be an approximation of the core evolution at higher densities and temperatures.

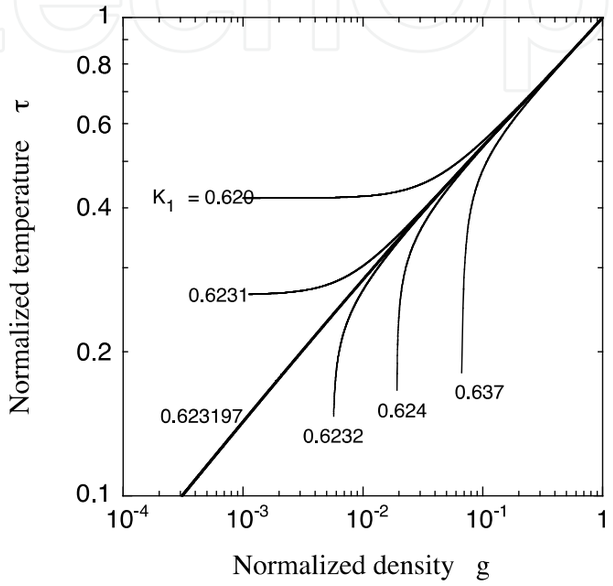


Fig. 7. g - $\tau$ diagram showing the optimization process of the eigenvalue, $K_1$.

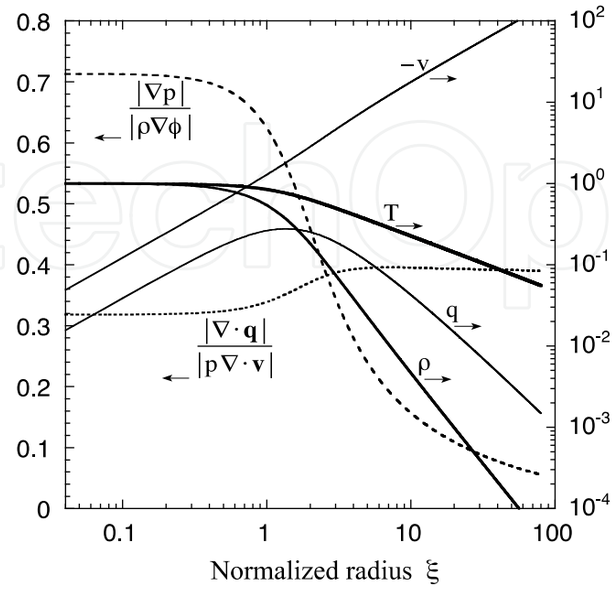


Fig. 8. Eigenstructure of the self-similar solution.

Under the condition that the right integrated curve is to converge to $g = \tau = 0$, each curve has already optimized with respect to $K_2$ as was shown in Fig. 6. Other fixed parameters are the same as in Fig. 6.
The normalized physical quantities are obtained as a result of the two-dimensional eigenvalue problem with fixed parameters, $m = 2$, $n = 13/2$, and $\gamma = 5/3$.

## 5. Conclusions

The crucial role of dimensional analysis and self-similarity are discussed in the introduction and the three subsequent examples. Self-similar solutions for individual cases have been demonstrated to be derivable by applying the Lie group analysis to the set of PDE for the hydrodynamic system, taking nonlinear heat conductivity into account as the decisive physical ingredient. The scaling laws for thermally conductive fluids are conspicuously different from those for adiabatic fluids (not discussed in the present chapter; see references by Murakami et al., 2002, 2005 for details). The former has one freedom less than the latter due to the additional constraint of thermal conductivity. If a thermo-hydrodynamic system comprises multiple heat conduction mechanisms, self-similarity cannot be expected in a vigorous sense except for special cases. However, self-similarity and scaling laws can always be found at least in an approximate manner, by shedding light on the dominant conduction mechanism, which should give the basis of system design and diagnostics for scaled experiments for individual cases. The necessity of dimensional analysis and finding self-similar solutions is encountered in many problems over wide ranges of research. The simple general scheme and the examples mentioned in this chapter will help the reader who encounters a similar situation in his or her investigation find the underlying physics and prepare further theoretical and experimental setup.

## 6. References

Antonova, R.N. & Kazhdan, Y.M. (2000). "A self-similar solution for spherically symmetric gravitational collapse " *Astronomy Letters*, Vol. 26, pp. 344 - 355.

Barenblatt, G.I. (1979). *Similarity, Self-Similarity, and Intermediate Asymptotics* (New York: Consultants Bureau).

Basko, M.M. & Murakami, M., (1998). "Self-similar implosions and explosions of radiatively cooling gaseous masses" Phys. Plasma, Vol. 5, pp. 518 – 528.

Bernstein, I.B. & Book, D.L. (1978). "Rayleigh-Taylor instability of a self-similar spherical expansion" *Astrophysical Journal,* Vol. 225, pp. 633 – 640.

Gitomer, S.J.; Morse, R.L. & Newberger, B.S. (1977). "Structure and scaling laws of laser-driven ablative implosions", Phys. Fluids Vol. 12, pp. 234 - 238.

Guderley, G. (1942) "Starke kugelige und zylindrische Verdichtungsstöße in der Nähe des Kugelmittelpunktes bzw. der Zylinderachse" Luftfahrtforschung Vol. 19, pp. 302–312.

Gurevich, A.V.; Parrska, L.V. & Pitaevsk, L.P. (1966). "Self-similar motion of rarefied plasma" *Sov. Phys. JETP*, Vol. 22, pp. 449 - &.

Kull, H.J. (1989). "Incompressible Description of Rayleigh-Taylor Instabilities in Laser-Ablated Plasmas" *Phys. Fluids,* Vol. B1, pp.170 - 182.

Kull, H.J. (1991). "Theory of Rayleigh-Taylor Instability" *Phys. Reports,* Vol.206, pp.197 - 325.

Landau, L.D. & Lifshitz, E.M. (1959). *Fluid Mechanics* (New York: Pergamon).

Larson, R.B. (1969). "Numerical calculations of the dynamics of collapsing proto-star" *Mon. Not. R. Astr. Soc.*, Vol. 145, pp. 271-&.

Lie, S. (1970). *Theorie der Transformationsgruppen* (New York: Chelsea).

London, R.A. & Rosen, M.D. (1986) "Hydrodynamics of Exploding Foil X-ray Lasers" Phys. Fluids, Vol. 29, pp. 3813 - 3822.

Mora, P. (2003). "Plasma Expansion into a Vacuum" Phys. Rev. Lett. Vol.90, 185002 (pp. 1 - 4).

Murakami, M.; Meyer-ter-Vehn, J. & Ramis, R. (1990). "Thermal X-ray Emission from Ion-Beam-Heated Matter" J. X-ray Sci. Technol., Vol. 2, pp. 127 - 148.

Murakami, M. & Meyer-ter-Vehn, J. (1991) "Indirectly Driven Targets for Inertial Confinement Fusion" *Nucl. Fusion*, Vol. 31, pp. 1315 – 1331.

Murakami, M., Shimoide, M., and Nishihara, K. (1995). "Dynamics and stability of a stagnating hot spot" *Phys. Plasmas*, Vol.2, pp. 3466 - 3472.

Murakami, M. & Iida, S., (2002). "Scaling laws for hydrodynamically similar implosions with heat conduction", *Phys. Plasmas*, Vol.9, pp.2745 - 2753.

Murakami, M.; Nishihara, K. & Hanawa, T. (2004). "Self-similar Gravitational Collapse of Radiatively Cooling Spheres", *Astrophysical Journal*, Vol. 607, pp.879 - 889.

Murakami, M.; Kang, Y.-G.; Nishihara, K.; Fujioka, S. & Nishimura, H. (2005). "Ion energy spectrum of expanding laser-plasma with limited mass", *Phys. Plasmas,* Vol.12, pp. 062706 (1-8).

Murakami, M. & M. M. Basko (2006). "Self-similar expansion of finite-size non-quasi-neutral plasmas into vacuum: Relation to the problem of ion acceleration", *Phys. Plasmas*, Vol. 13, pp. 012105 (1-7).

Murakami, M.; Fujioka, S.; Nishimura, H.; Ando, T.; Ueda, N.; Shimada, Y. & Yamaura, M. (2006). "Conversion efficiency of extreme ultraviolet radiation in laser-produced plasmas", *Phys. Plasmas*, Vol.13, pp. 033107 (1-8).

Murakami, M.; Sakaiya, T. & Sanz, J. (2007). "Self-similar ablative flow of nonstationary accelerating foil due to nonlinear heat conduction", *Phys. Plasmas*, Vol. 14, pp. 022707 (1-7).

Pakula, R. & Sigel, R., (1985). "Self-similar expansion of dense matter due to heat-transfer by nonlinear conduction " *Phys. Fluids,* Vol. 28, pp. 232 - 244.

Penston, M.V. (1969). "Dynamics of Self-Gravitating Gaseous Spheres – III Analytical Results in the Free-Fall of Isothermal Cases" *Mon. Not. R. astr. Soc.*, Vol. 144, pp. 425 - 448.

Sedov, L.I. (1959). *Similarity and Dimentional Methods in Mechanichs* (New York : Academic).

Sanz, J.; Nicolás, J.A.; Sanmartín, J.R. & Hilario, J. (1988). "Nonuniform target illumination in the deflagration regime: Thermal smoothing", *Phys. Fluids,* Vol. 31, pp. 2320 – 2326.

Takabe, H; Montierth, L. & Morse, R.L. (1983). "Self-consistent Eigenvalue Analysis of Raileigh-Taylor Instability in an Ablating Plasma", *Phys. Fluids*, Vol. 26, pp. 2299 - 2307.

True, M.A.; Albritton, J.R. & Williams, E.A. (1981). "Fast Ion Production by Suprathermal Electrons in Laser Fusion Plasmas", *Phys. Fluids* Vol. 24, pp. 1885 - 1893.

Zel'dovich, Ya.B. & Raizer, Yu.P. (1966). *Physics of Shock Waves and High Temperature Hydrodynamic Phenomena* (New York: Academic Press).

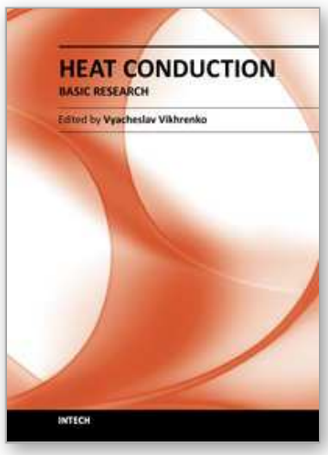


**Heat Conduction - Basic Research**

Edited by Prof. Vyacheslav Vikhrenko

ISBN 978-953-307-404-7
Hard cover, 350 pages
**Publisher** InTech
**Published online** 30, November, 2011
**Published in print edition** November, 2011

The content of this book covers several up-to-date approaches in the heat conduction theory such as inverse heat conduction problems, non-linear and non-classic heat conduction equations, coupled thermal and electromagnetic or mechanical effects and numerical methods for solving heat conduction equations as well. The book is comprised of 14 chapters divided into four sections. In the first section inverse heat conduction problems are discuss. The first two chapters of the second section are devoted to construction of analytical solutions of nonlinear heat conduction problems. In the last two chapters of this section wavelike solutions are attained.The third section is devoted to combined effects of heat conduction and electromagnetic interactions in plasmas or in pyroelectric material elastic deformations and hydrodynamics. Two chapters in the last section are dedicated to numerical methods for solving heat conduction problems.



**InTech Europe**
University Campus STeP Ri
Slavka Krautzeka 83/A
51000 Rijeka, Croatia
Phone: +385 (51) 770 447
Fax: +385 (51) 686 166
www.intechopen.com

**InTech China**
Unit 405, Office Block, Hotel Equatorial Shanghai
No.65, Yan An Road (West), Shanghai, 200040, China
中国上海市延安西路65号上海国际贵都大饭店办公楼405单元
Phone: +86-21-62489820
Fax: +86-21-62489821

IntechOpen